Optical Constants Correlated Electrons-Spin of Micro Doughnuts of Mn-doped ZnO films

S.S Nkosi[1,2,3], I. Kortidis[4], D.E. Motaung[3,*], J. Keartland[2], E. Sideras-Haddad[2,†], A. Forbes[1,2], B.W. Mwakikunga[3,‡], G. Kiriakidis[4], S. Sinha-Ray[3]

[1]CSIR-National Laser Centre, 627 Meiring Naude Rd, Brummeria, Pretoria 0001, RSA

[2]School of Physics, University of Witwatersrand, Private Bag X3, Johannesburg 2030, RSA

[3]DST/CSIR Nanotechnology Innovation Centre, National Centre for Nano-Structured Materials, Council for Scientific and Industrial Research, P.O. Box 395, Pretoria, 0001, RSA

[4]Transparent Conductive Materials Lab, Institute of Electronic Structure and Laser, Foundation for Research and Technology Hellas, 100 N. Plastira str., Vassilika Vouton, 70013 Heraklion, Crete, Greece

ABSTRACT

Diluted magnetic semiconductor (DMS) Mn:ZnO thin films with “ring-like or doughnut-like” structures were grown using aerosol spray pyrolysis for 20 and 30 min. Electron paramagnetic resonance revealed the ferromagnetic ordering which varies with Mn concentration. These ferromagnetic films obtained coexist with dielectric state. Spectroscopic ellipsometry results showed that the dielectric constants ε_1 and ε_2 also vary in definite pattern as Mn concentration. We used and fitted Bruggeman theory to explain these trends and to find ε_1 and ε_2 for both ZnO and Mn which compare well with literature. The results showed that the structural,

* Corresponding Author: Dr. David Motaung;
E-mail: dmotaung@csir.co.za; Tel.: (+27)12-8414775
† Corresponding Author: Prof. Elias Sideras-Haddad;
E-mail: elias.Sideras-Haddad@wits.ac.za
‡ Corresponding Author: Dr. Bonex Mwakikunga;
E-mail: bmwakikunga@csir.co.za; Tel.: (+27)12-8414771

optical and magnetic properties of these DMSs are strongly sensitive to the preparation parameters. It is unambiguously demonstrated that the room-temperature ferromagnetism is strongly correlated with dielectric constants. The Effective medium approach Bruggeman model used to fit our experimental data demonstrated a decrease in the dielectric constant with the addition of Mn concentration. These findings revealed that the refractive index of the films increases with ferromagnetic ordering while the extinction coefficient reduces. This indicates that when the Mn:ZnO film becomes more opaque (high reflecting) to UV (~ 370 nm) and absorbs less of that light, the ferromagnetic ordering is enhanced. A relatively new phenomenon of *d*-band resonance at 3.35 eV (~ 370 nm polarized light) from Zn-O:O-Mn molecule at 0.25 at. % Mn was observed for both 20 (thinner film) and 30 minutes (thicker film) deposited Mn:ZnO films. A good correlation between ferromagnetic intensity signal with its width and angular dependence for the films was also observed.

Keywords: Aerosol spray pyrolysis; Zinc oxide; DMS; Optical constants; EPR

1. INTRODUCTION

Diluted magnetic semiconductors (DMSs) have attracted intense interest due to their potential applications such as spintronics devices which utilize both the charge and spin of electrons to create new functionalities beyond conventional semiconductors **[1-3]**. DMSs are semiconductor solid solutions, where a small percentage of cations are replaced by magnetic impurities such as Mn. Due to the host sp-Mn d interactions in these DMSs, ferromagnetism can be produced **[3, 4]**.

The main challenge for this kind of novel materials is to preserve their magnetic character at room temperature and above in order to be useful for technological applications. According to the ferromagnetic exchange coupling theory, an ideal DMS should have a homogeneous distribution of the magnetic dopants. The presence of any magnetic precipitate in the host semiconductors in the form of secondary phases of the magnetic impurities is detrimental to the real applications of DMSs and therefore should be avoided **[5]**. In the exploration of the specific materials, zinc oxide (ZnO) has been identified as an excellent candidate host semiconductor for supporting room-temperature ferromagnetism when doped with variety of 3d transition metal ions, particularly Mn^{2+} **[6]**. Scientists have verified these predictions in some cases, with ferromagnetism above room-temperature reported for ZnO doped with cobalt (Co) **[7]**, iron (Fe) **[8]** and vanadium (V) **[9]**, prepared by vacuum deposition methods such as pulsed laser deposition (PLD). Room-temperature ferromagnetism for Mn doped ZnO was first reported by Sharma et al. **[10, 11]**, even though this DMS was specifically highlighted in theoretical studies for its high-T_c (Curie temperature) ferromagnetism potential **[6]**.

This led to these p-conducting III-V and II-VI DMS being studied due to their wide band gap energies as prospective DMSs for achieving magnetic ordering at ambient temperatures and above. For example a Curie temperature above room-temperature, 940 K, has been reported for these p-conducting (Ga, Mn)N **[12]**. Since metallic manganese (Mn) is paramagnetic, any ferromagnetism detected in Mn doped ZnO cannot be due to Mn clusters formed during the growth process. Ferromagnetism near or above room temperature has already been reported for Mn-doped ZnO nanocrystals, pellets and thin films **[10, 13-14]**, whereas in other studies

only paramagnetic behaviour was reported **[15-17]** among others. However, in all these previous works, it has been difficult to implement homogeneous doping through various fabrication approaches. In the same area of ferromagnetism, a relatively new phenomenon called “low-field microwave absorption” has been observed in ferromagnetic materials and other various materials such as high temperature superconductors, ferrites, manganites, doped silicate glasses and soft magnetic materials. Different interpretations have been put forward to try and explain this phenomenon.

Recently, Xu et al. **[18]** and Coey et al. **[19]** showed that the undoped ZnO exhibit intrinsic room temperature ferromagnetism. This finding shed more light on the ideas and the observations that the room temperature ferromagnetism is due to the dopant carrier in ZnO materials. They showed that defects related to oxygen vacancies (V_o) and zinc interstitials clusters are magnetic. Probably the dopants in ZnO induce the ferromagnetism along with defects in the ZnO structure. It is worth pointing out that a large number of edge dislocations, which were directly observed by HRTEM, enhanced the concentration of V_o and/or Zn_i point defects, and thus increased the room temperature ferromagnetism intensity of transition metal doped ZnO films **[20, 21]**. As mentioned earlier, substitution of transition metal ions are necessary but not sufficient condition for ferromagnetism ordering and large variations in carrier concentration and magnetic properties have been reported for otherwise similar samples, indicating a strong dependence of room temperature ferromagnetism on the synthesis and processing parameters **[22, 23]**. It is therefore important to design a series of experiments to distinguish the variation of carriers and structural defects and thus to identify the nature of the room temperature

ferromagnetism. Without any loss of generality, we shall consider the study of the effective dielectric constants for a system made up of spherical multicomponent inclusions with different arbitrary dielectric constants. The properties under consideration are usually the conductivity σ or the dielectric constant ε of the medium. These parameters are interchangeable in the formulas in a whole range of models due to wide applicability of the Laplace equation. These effective medium approximations physical models describe the macroscopic properties of a medium based on the properties and relative fractions of its components. Then the Bruggeman formula takes the form:

$$\sum_i \delta_i \frac{\varepsilon_i - \varepsilon_{eff}}{\varepsilon_i + (n-1)\varepsilon_{eff}} = 0 \qquad (1)$$

In a system of Euclidean spatial dimension *n* that has arbitrary number components **[24]**, the sum is made all over the constituents. δ_i and ε_i are respectively the fraction and the dielectric constant of each component, and ε_{eff} is the effective dielectric constant of the medium. (The sum over the δ_i's is unity.)

In this work, an aerosol spray pyrolysis (ASP) technique was used for preparation of metal oxide nano-materials due to its advantages of implementation of doping at the same time of metrical crystal growth process. This technique has been used to produce good ZnO nanostructures for photo-catalytic and gas sensing application **[25-27]**. Herein we report on the observation of room-temperature ferromagnetism of Mn doped ZnO films grown by ASP at various Mn atomic percentages and deposition times (20 min and 30 min) (thin and thick films) correlated to dielectric constants. An observation by spectroscopic ellipsometry

revealed that the dielectric constant varies in definite pattern with Mn concentration. We discuss the observed correlation between the number of spins and the dielectric constant. Interestingly, these films possess some low-field magnetic features. Furthermore, angular dependence of the ferromagnetism in Mn doped ZnO films together with the low-field magnetic anomalies are also studied. The structural, morphological and optical properties of the undoped and Mn doped ZnO DMS materials are also investigated in detail. Additionally, surface analysis reveals that Mn:ZnO films contain “ring-like or doughnut-like” structures.

2. EXPERIMENTAL DETAILS

2.1 Synthesis of undoped and Mn doped ZnO films grown by aerosol spray pyrolysis

The undoped and Mn doped ZnO films were fabricated in a home-made aerosol spray pyrolysis system **[18, 25]**. The spray solution was prepared by dissolving appropriate volumes of solution containing 0.1 M zinc nitrate dehydrate $Zn(NO_3)^2$ (purity > 99%, Sigma-Aldrich) and different dopant concentrations of Mn (0.1, 0.25, 0.5, 1, and 2 at.%) in distilled water. The solutions were stirred at room temperature for a few minutes to yield a clear and homogeneous solution. The films were deposited at a constant flow rate of 300 ml h^{-1} by means of a nozzle assisted by a nitrogen carrier gas at 0.5 bar, over a heated corning glass substrate. The distance between the tip of the nozzle and the substrate was kept at 28 cm. The atomization of the solution in the fine droplets was affected by spray nozzle with the help of compressed air, during the course of spray. The average diameter of the

misted droplet generated from the vibration of the transducer can be approximately calculated from an expression given as **[28]**;

$$D_{drop} = 0.34\left(\frac{8 \cdot \pi \cdot \gamma}{\rho \cdot f^2}\right)^{1/3} \quad (2)$$

where, D_{drop}, is the expected diameter of the droplet diameter (μm), γ, the solution surface tension (σ = 69.6 $g.cm^{-1}s^{-2}$), ρ, the liquid density (ρ = 1$g \cdot cm^{-3}$) and f, the frequency of the transducer (*f* = 1.8 MHz). The solvent diameter of the resulting ZnO particles, D_{ZnO}, can be estimated from Kelvin's relation **[29]** to be around D_{ZnO} = 0.31μm.

$$D_{ZnO} = \left(\frac{M_{ZnO} \cdot C}{\rho_{ZnO}}\right)^{1/3} \cdot D_{drop} \quad (3)$$

where, M_{ZnO} is the molecular weight of ZnO and ρ_{ZnO} is the density of ZnO. The un-doped and Mn doped ZnO films were deposited for 20 and 30 min at a substrate temperature of 350 ˚C. It is worthy to point out that the films deposited for 20 min resulted to thinner films while the 30 min deposited films resulted to thicker films in spite of Mn concentration. Temperature of the heating plate and substrate was recorded by a K-type thermocouple and controlled by a Eurotherm400 temperature controller. All the films have been prepared by varying the Mn concentration. Prior to deposition, corning 1737 F glass substrates (25.4×25.4 mm^2) were ultrasonically cleaned with acetone, ethanol and deionized water.

2.2 Characterization

To study the surface morphology, polarized optical microscope (POM) technique was used. Thin films were placed between two covering glasses and placed on a Linkam hot-stage (Linkam Scientific Instruments Ltd, UK), mounted on a POM instrument. Raman spectra were collected using a Horiba Jobin-Yvon HR800 Raman microscope equipped with an Olympus BX-41 microscope attachment. An Ar^+ laser (514.5 nm) with energy setting 1.2 mW from a Coherent Innova Model 308 was used as an excitation source. The Variable angle spectroscopic ellipsometry (VASE) spectra (Ψ) and (Δ) were obtained in the range of 250-1000 nm at room temperature by using a rotating-compensator instrument (J.A. Woollam, M-2000) at multi-angles of incidence (AOI) (65, 70 and 75°). For clarity we displayed spectra only at 75° AOI since they behave similarly at different AOI. The films were regarded as a homogeneous material with film thickness modelled using Cauchy model **[30]**. A *B-Spline* model **[31, 32]** was then used to extract the refractive index (n) and extinction coefficient (k) over the absorption range from 300 to 900 nm. Employing the ellipsometric parameters (Ψ) and (Δ), the thickness, refractive index (n) and the extinction coefficient (k) of the unknown layer onto known substrate could be extracted. The microwave absorption measurements were carried out using JEOL electron spin resonance (ESR) spectrometer operated at 9.4 GHz (x-band). For the analysis, the films were mounted in the cavity centre at position where the microwave magnetic field is the maximum. The DC static field H_{DC} was slowly swept between 0 and 500 mT. The microwave power was kept at 5 mW to avoid saturation. The DC field was modulated with a superposed ac field whose amplitude was varied between 1 mT and 6 mT at 100 kHz frequency. The microwave response was

measured as a derivative of microwave absorption signal. It should be pointed out that the measurements were carried out at room temperature (298 K).

3. RESULTS AND DISCUSSION

Fig. 1 shows the optical microscopy micrographs of Mn (2at. %) doped ZnO films deposited for 20 and 30 min by spray pyrolysis. It is shown in Fig. 1a that the thinner film deposited for 20 min, shows “ring-like” structures that are attached to each other with diameters ranging from 80 to 150 μm. The thicker film deposited for 30 min, Fig 1b, shows more concentrated “ring or sphere-like” structures that are covering the entire film surface with diameters much smaller than their counterparts.

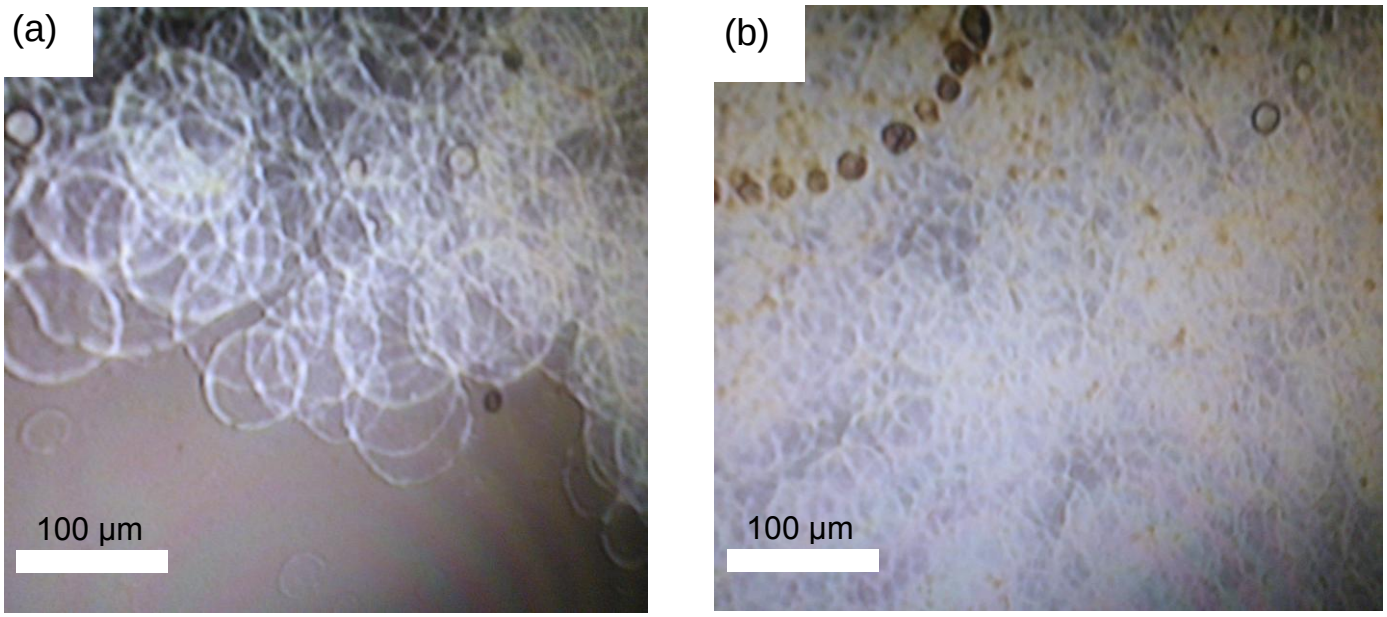

Fig. 1: The optical microscope images for the Mn (2 at.%) doped ZnO structures with different films (a) thinner and (b) thicker films.

For a systematic and more detailed optical imaging of these structures, polarized optical microscopy analysis was performed on various films. For the thinner film, as shown in Fig. 2a, it is noticed that at lower concentration, 0.1 at.% Mn, no “ring-like” spheres are observed on the film surface. However, at 0.5 at.% Mn, (Fig. 2b) the formation of “ring-like” structures become visible across the film with small diameters in the range of 5-20 µm. A change in colour contrast is also observed for these films depending on the carrier concentration of Mn.

The micrograph in Fig. 2c shows that upon increasing the Mn doping level to 2 at.% Mn, these “ring-like” structures become more visible throughout the film. It is evident that these structures are due to the presence of Mn. Both thinner and thicker films of the un-doped ZnO films did not show any of these structures or features **[33]**. The thicker film with a doping concentration of 0.1% Mn, shows an abundant amount of these “ring or sphere-like” structures which are clustered together. Increasing the doping level of Mn to 0.5 at.%, a dark visible spots forming circular orientations across the film are observed. These dark visible spots diminish at higher Mn concentration (2 at.% Mn), forming thicker circular orientations with much bigger diameters (Fig. 2f). This points out that the diameters of these structures are depending more on the Mn concentration.

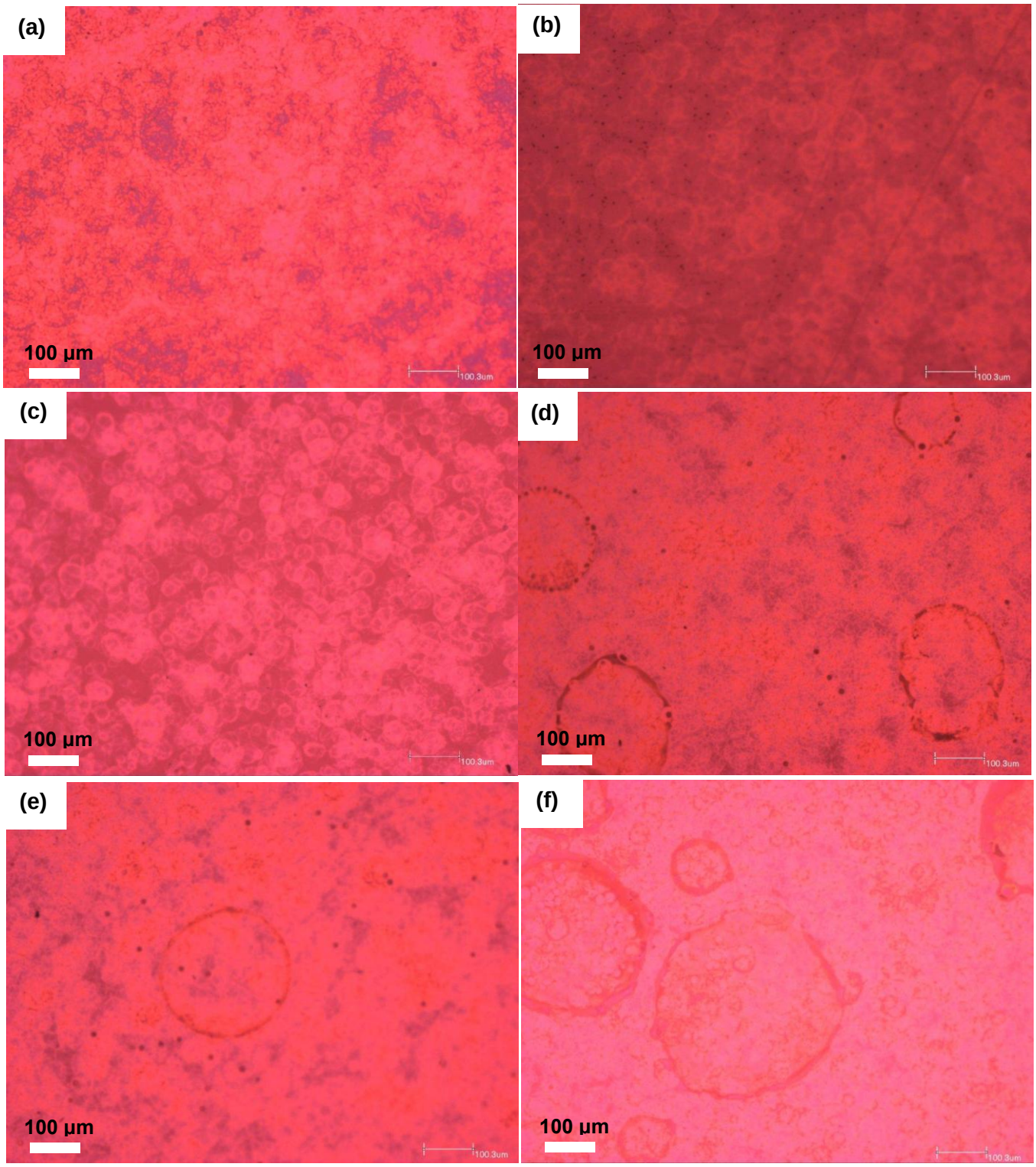

Fig. 2: Polarized optical microscope images of Mn doped ZnO structures of thin (a-c) and thick films (d-f). The Mn concentrations used were 0.1, 0.5 and 1at.% for both thinner and thicker films.

Fig. 3 shows SEM micrographs of undoped and Mn doped ZnO films deposited at different film thicknesses as indicated earlier. The undoped ZnO with a thinner film shows well adherent and smooth film with smaller ZnO particles ranging from 5 to 10 nm (Fig. 3a). Upon introducing the 0.1 at.% of Mn (Fig. 3b) in the ZnO matrix, the “ring or sphere-like” structures as seen by the optical microscopy are now appearing as “doughnuts-like” or “ring-like” structures with thick edges across the film in SEM. By using the in-lens detector (high magnification) in the SEM, the edge of these “doughnuts-like” contains nanoparticles which are 30-50 nm in diameter range (Fig3b, inset). When increasing the Mn (1 at.%) further (Fig. 3c), the diameter of the doughnuts or rings structures reduce, while their edges becomes thicker. At higher magnification as shown in the inset of Fig. 3c, the particle size increases with an increase in Mn dopant at the edge of the doughnut and are more compact. Fig. 3d shows the undoped ZnO nanorods with a thicker film. The results show that ZnO nanorods are grown perpendicular to the substrate, entangled to one another forming “spaghetti-like” structures. These “spaghetti-like” structures were previously observed in our SEM results with an average diameter in the range of 25-35 nm **[31]**. Again, when Mn ions (0.1 at.%) are inserted in the host matrix, still “doughnuts-like” structures are preserved with diameter ranging from 20 to 40 µm. The higher magnification analysis (see inset, Fig.3e) shows an alteration on the surface morphology as compared to the undoped ZnO (Fig. 3d). We observed formation of nanoparticles rather than the “spaghetti-like” structures. The inset of Fig. 3f shows that the size of the nanoparticles decreases further with an increase in Mn doping level (1 at. %). This comes with an increase in the doughnuts diameters as evident in (Fig.3f) SEM image.

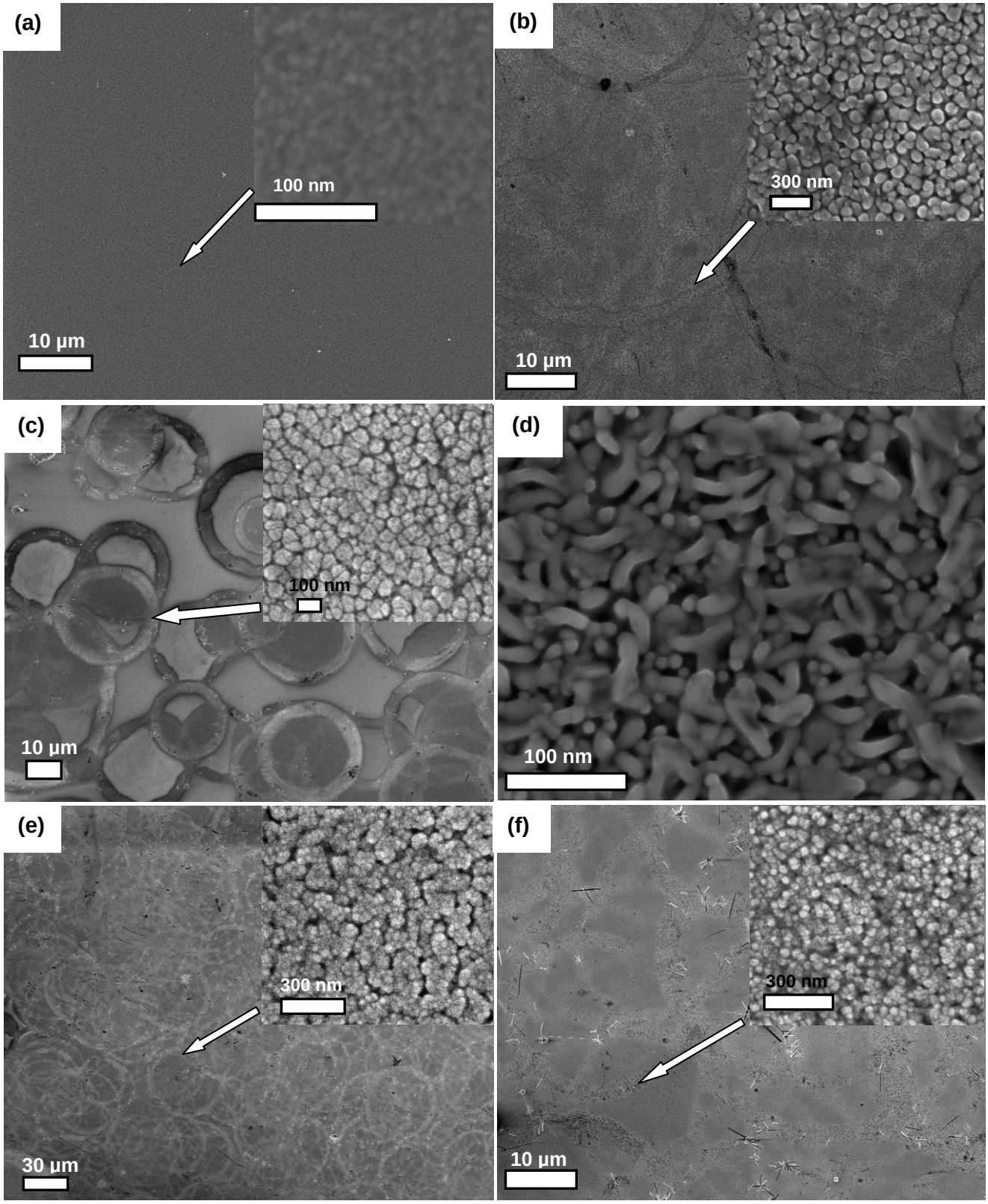

Fig. 3: SEM micrographs of (a) undoped ZnO with a thinner film, (b) 0.1at.%, (c) 1at.% Mn doped ZnO with thinner films; (d) undoped ZnO with a thicker film, (b) 0.1at.%, (c) 1at.% Mn doped ZnO with thicker films.

Therefore, the incorporation of Mn does not only promote formation of the doughnuts but also completely modify the ZnO structure. This is consistent with our atomic force microscopy (AFM) analysis, where the surface roughness of the thinner films increases, while it decreases for thicker films with Mn concentration (results not shown). We believe that the nature of the growth process adopted by the present experimental set-up which points out that the observed irregularities are characteristic of the ultrasonic nature of the atomization process and the thermodynamic environment as the droplets strike the substrate. More specifically, we attribute the early stage irregularities with the thermal gradient and the repelling thermophoretic forces on the on-coming droplets from the high temperature (350˚C) substrate particularly for droplets smaller than 2 μm diameters that experience a very high evaporation rate. However, as the deposition process proceeds, the temperature gradient and the evaporation rate get reduced and spreading of droplets prevails **[34, 35]**. These processes may explain the observed significant variations in the film structure. We performed an electron backscattering measurements (EBS) to investigate whether these “doughnut-like” structures are of different phases. The electron backscattered analysis shown in Fig 4 also confirms the formation of “doughnut or ring like” structures. The results in Fig. 4a and b denote that both thinner and thicker films have two phases, 1 and 2 as indicated in Fig. 4a. This suggests that phase 2 is highly concentrated with the Mn:ZnO materials than phase 1. Energy dispersive x-ray spectroscopy (EDS) mapping (see Fig. S1 of the supplementary information) showed that Mn is homogenously distributed in a proportional ratio throughout the film without showing any clusters.

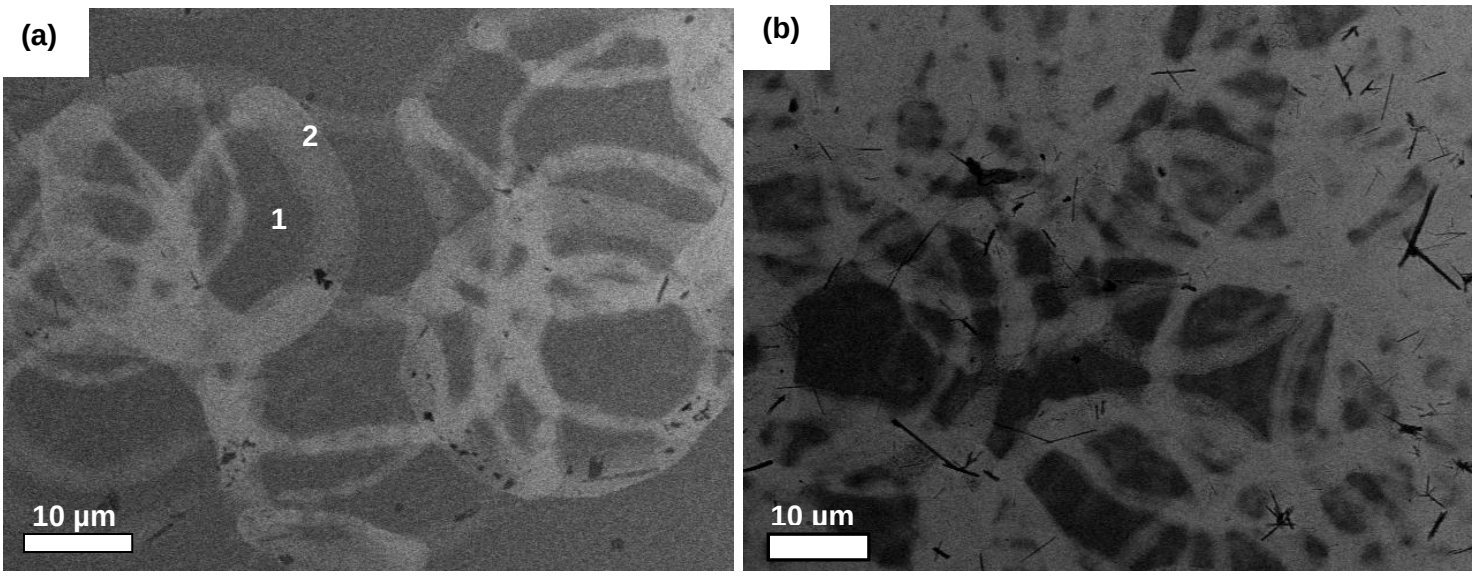

Fig. 4: EBS-Detector micrographs of Mn doped ZnO (1 at.%) with thinner and thicker films deposited for (a) 20 min and (b) 30 min indicate different phases on the surface of Mn:ZnO films.

Fig. 5 shows the Raman scattering spectra of the Mn: ZnO with thinner and thicker films deposited for (a) 20 and (b) 30 min, respectively measured at room temperature. The Mn ions induce disorder even if perfectly incorporated on Zn sites, inherent to the mixture of Zn and Mn on the cation sub-lattice. The origin of these features, such as isolated impurity modes, disorder-induced silent modes, or phonon modes by precipitates, is still controversial. Table 1 shows the summary of phonons observed for both thinner and thicker films. It is observed from Fig. 5 and Table 1 that the FWHM of the E_{2H} for both films reduces with increasing Mn concentration. This is probably due to the suppression of the ZnO sub-lattice induced by incorporation of Mn^{2+} into Zn^{2+} host matrix. The slight shift in E_{2H} modes to higher wavenumber Δv (cm^{-1}) is due to non-stoichiometry and strain effects. The red-shifting normally indicates tensile strain of the oxides. The high and low Raman

intensities of the vibrational modes are indicative of donor defects-induced into the ZnO system. The intrinsic lower intensity, regardless of Mn concentration, of the vibrational modes at 1439 cm^{-1} for both thinner and thicker films indicates optical overtones process and is associated with the 2^{nd} order Raman active modes. The vibrational modes at 790 and 1081 cm^{-1} especially for the thicker films which is due to longitudinal acoustic and transverse-optical (LA+TO) and transverse optical and longitudinal optical stretching modes (TO+LO) respectively are defect related. It can be noticed that the modes phonon at 790 cm^{-1} (LA+TO) is suppressed upon addition of Mn. It is also observed that the vibrational modes at 1081 cm^{-1} (TO+LO) enhances upon the addition of Mn concentration. Similarly for the thinner films, the same vibrational modes at 1091 cm^{-1} which is red-shifted for the thicker films enhances on increasing the Mn concentration. We can conclude that it is due to the present of Mn on Zn sub-lattice. However this 1091 cm^{-1} mode is more resolved and excited, higher in intensity on the thinner films than on the thicker films which appears to be suppressed or less excited. The Raman phonon intensification and broadening are an effect of disorders created during growth and the incorporation of Mn with the local structure. Extrinsic Fröhlich scattering should not be overlooked especially for the longitudinal optical modes.

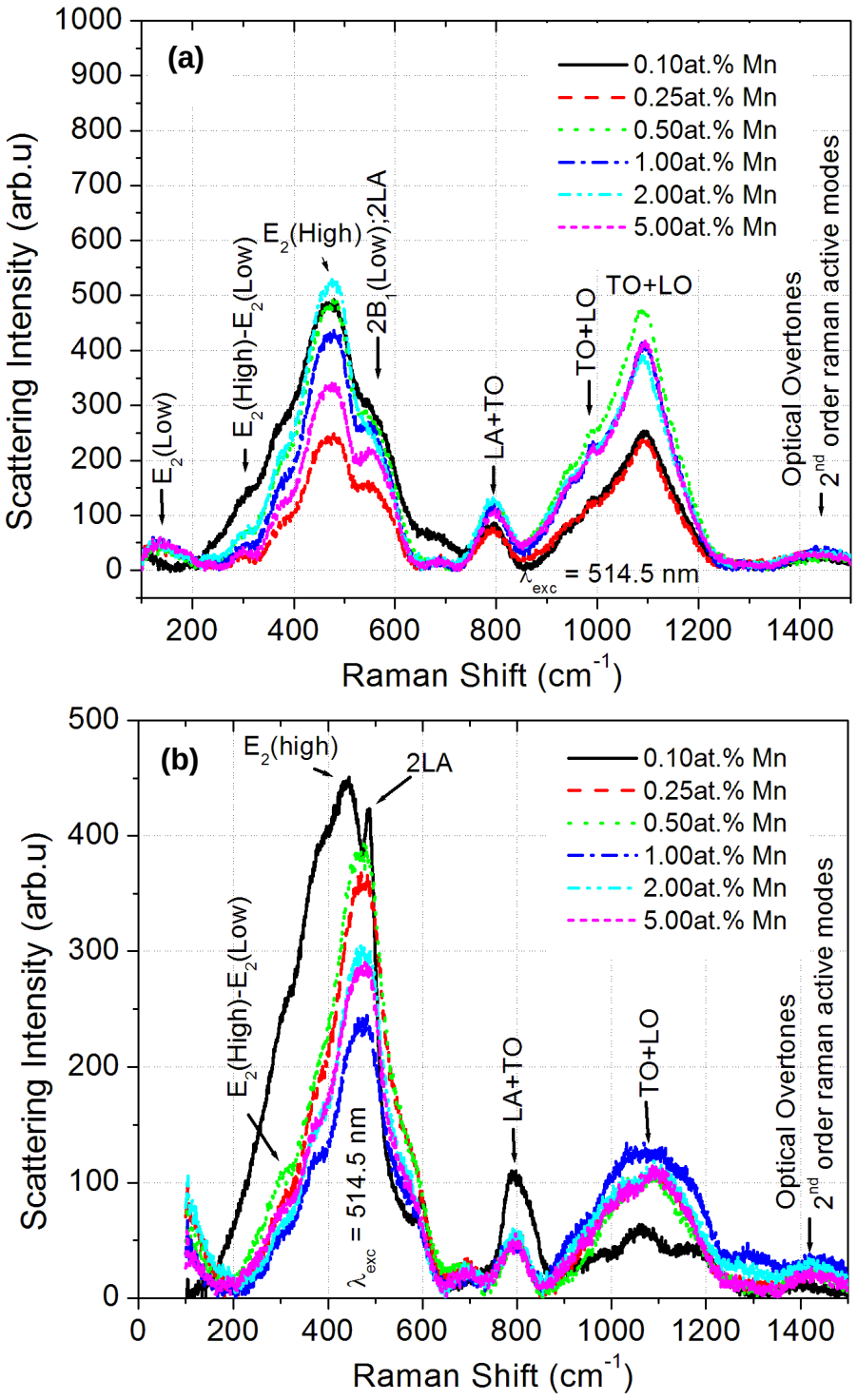

Fig. 5: Raman spectra of Mn:ZnO films at various concentration of Mn for both (a) thinner and (b) thicker deposited films respectively.

Defects and impurities magnetic correlation has been previously observed in many cases to help understand the nature and origin of RTFM more especially in these DMS/O systems. Previous results reported by Nkosi et al. **[36]** revealed that Mn doped ZnO films prepared by ASP possess three absorption peaks in associated with three processes: one centred at HDC ≈ 6 mT (low field signal), another at ~ 150 mT (paramagnetic feature) and lastly at ~ 300 mT (ferromagnetic field resonance). Ferromagnetic resonance (FMR) is due to the absorption in the full saturation state while the low field absorption process is usually originating from magnetization process far from the saturation state. These results confirmed the appearance of FMR at room temperature. Fig. 6 shows the effect of Mn concentration on the FMR intensity (extracted from FMR peaks) and peak-to-peak width (ΔH_{FMR}) at different film orientation to the applied magnetic field. In Fig. 6a, it is noticed that the FMR intensity signal is high at relatively low Mn concentration and reduces upon increasing the Mn doping in the host. A significant rise which is quite comparable to that of 0.1 at.% Mn is achieved at 5 at.% of Mn. Moreover, it is observed that the width (ΔH_{FMR}) also decreases when increasing Mn concentration. On the other hand when the films are titled normal to the applied field, the FMR intensity and the width (ΔH_{FMR}) signals decrease with an increase in Mn up to 2at. %. However, at higher Mn (>2at. %), both FMR intensity and the width (ΔH_{FMR}) signals increase as shown in Fig. 6b. It is observed from Fig 6c that the FMR intensity signal increases at higher Mn concentration (1-5 at. %), while width (ΔH_{FMR}) decreases. However, when the film is measured perpendicular to the field (90 $^{\circ}$), a similar behaviour is observed (Fig. 6d). This also is consistent with the surface morphology analyses.

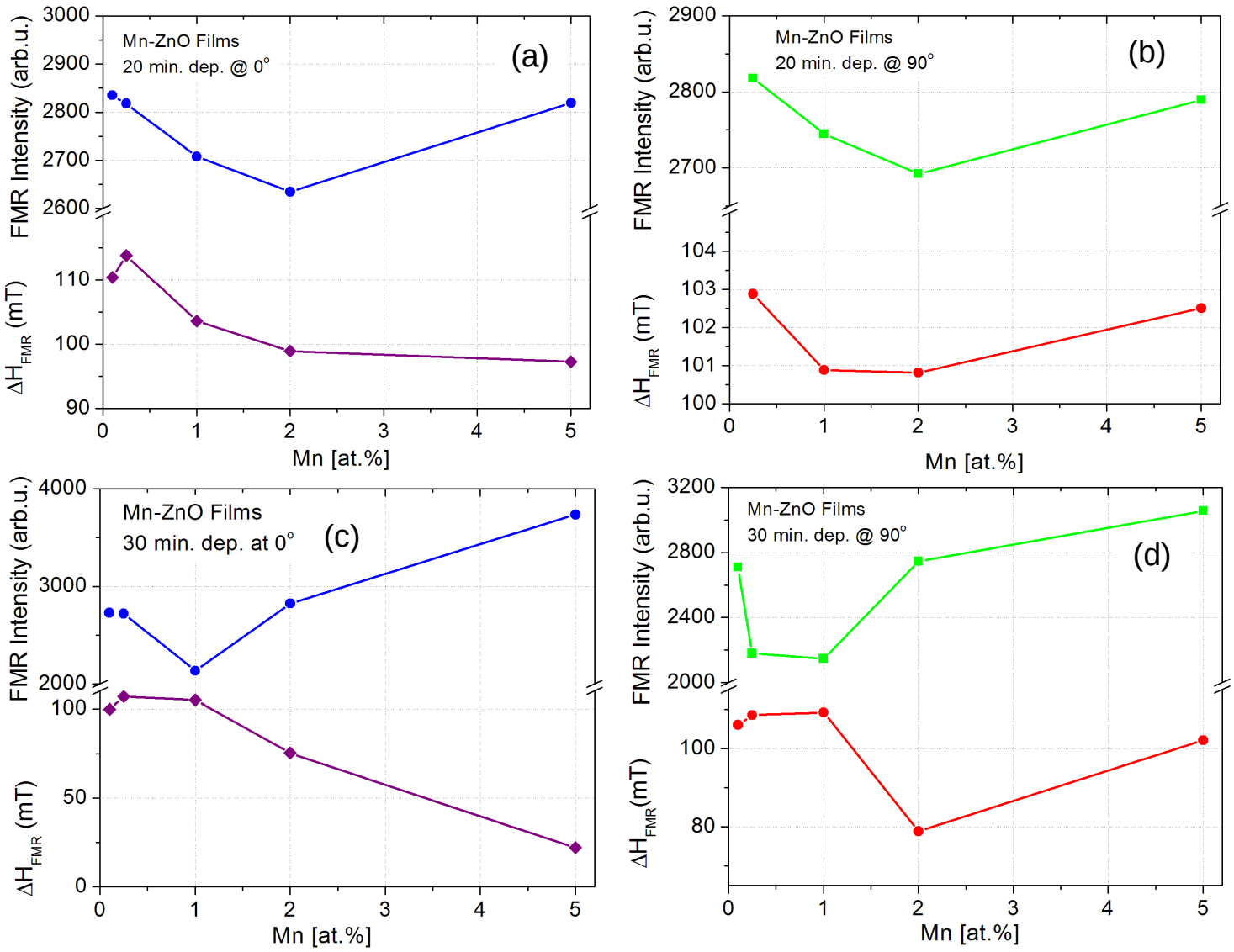

Fig. 6: The dependence of RTFM intensity and peak-to-peak width at various Mn concentrations (a) magnetic field parallel to the film and (b) when the magnetic field is perpendicular to the film. It should be pointed out that (a-b) correspond to the thinner films deposited for 20 min and (c-d) thicker films deposited for 30 min.

The increase in FMR intensity from 2 at% is due to the fact that the ferromagnetism signals transform to a sharper peak related to paramagnetism. This

indicates that a doping level of Mn 0.1-2 at.% results to FMR, while the doping level above 2 at.% resulting to a paramagnetism **[36]**. A similar transition has been observed by Nkosi et al. **[37]** for nickel oxide at room temperature induced by substrate annealing. Furthermore, upon increasing the doping level of Mn (5 at.%), the ferromagnetism completely disappears to another form of magnetism related to paramagnetic. The spins become randomly orientated at higher atomic percentages of Mn. Moreover, the optical constants (presented in Fig. 8) indicate an increase in refractive index and a decrease in extinction coefficient with increasing Mn concentration. This suggests that at higher Mn concentration the film become more reflective to the electromagnetic radiation. This alone, we believe could results in reduction in the magnetic ordering, ferromagnetism. However, Sharma et al. **[10]** reported that the decrease in ferromagnetic ordering above 2 % Mn doped ZnO films was attributed to Mn clustering which resulted in shorter Mn-Mn distances. This however is in contrast with the present study as evidenced by EDX mapping analysis (see supplementary information). It is further observed that the linewidth with the Mn concentration change decrease which could be due to an exchange narrowing of the ESR signal. However, the mechanism for intrinsic ferromagnetism in Mn-doped ZnO thin films still remains uncertain and therefore more work is in process for illustrating the fundamental physical processes in Mn-doped ZnO DMSs.

Fig. 7 shows the dependence of FMR spins with Mn concentration. It is noticed that the total number of spins for the thinner films deposited for 20 min reduce drastically with increasing the Mn concentration. However, the thicker films deposited for 30 min show an increase in number of spins at higher Mn concentration (1-2 at. %). This type of reversal behaviour at higher Mn concentration is consistent with

surface roughness and films thickness (results not shown). Since metallic Mn is paramagnetic, any ferromagnetism detected in Mn doped ZnO cannot be due to Mn clusters formed during the growth process. Therefore we expect to see a reduction in the number of spins with the addition of Mn. However, there exist some controversies on the origin of this RTFM in the diluted magnetic semiconductors **[22, 23, 38]**.

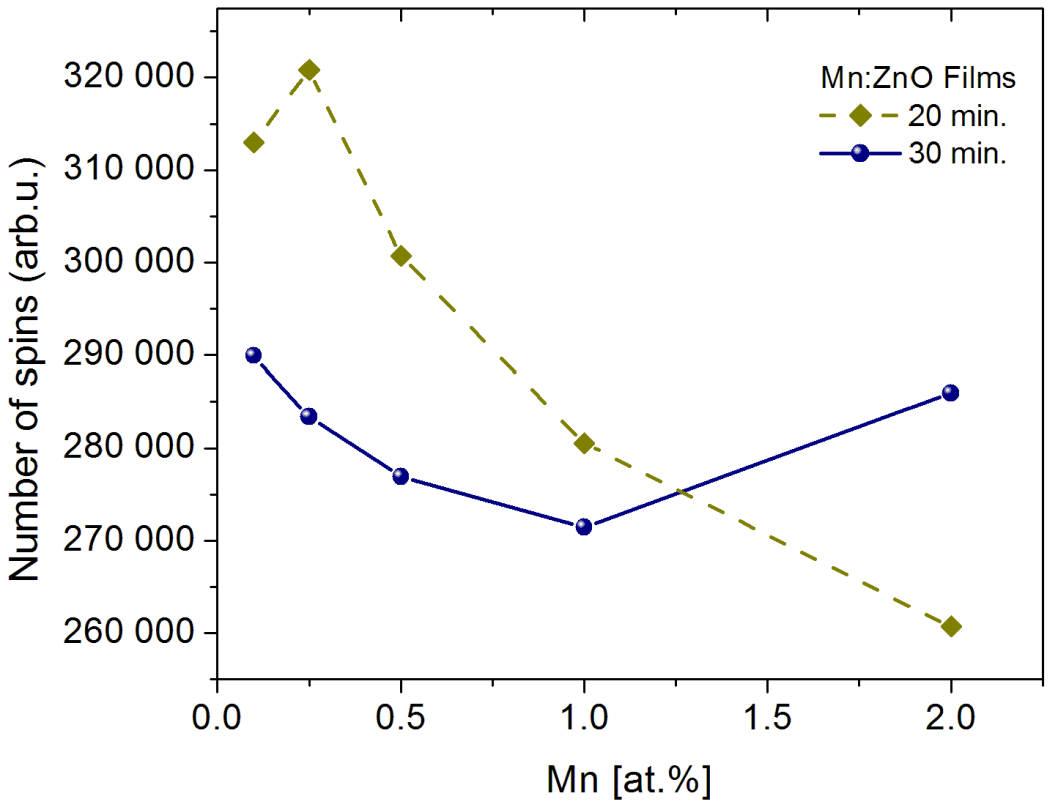

Fig. 7: The dependence of number of spins (N_s) of the ferromagnetic ordering as a function of Mn concentration.

Doped ZnO films are either conducting or semiconducting, as characterized by strong coupling between localized *d* electrons of the transition-metal ions and the ZnO structure characterized by highly dispersive-parabolic shape *s* orbitals of Zn and

rather localized with small dispersion *p* orbitals of O. Thus, the carriers are spin-polarized and can mediate ferromagnetism ordering of the magnetic moments of transition-metal ions doped into the oxide lattice i.e. transition-metal replace Zn^{2+} sites. Furthermore, additional electron doping, such as Co, Al, Sn, Cu, Ga, etc. to name a few, as well as hole doping, such as Co, Li, N, Mn, Fe, etc. has been investigated to further examine the carriers effect on RTFM **[39, 40]**. It was importantly noted that addition of carrier doping had no significant impact on RTFM enhancement and some films even showed RTFM with an inverse correlation between magnetization and electron density **[3, 41]**. Thus, inconsistent phenomena and conclusions have been obtained, indicating that the intrinsic RTFM of transition-metal doped ZnO systems remains a wide open question. It is hence of vital importance to clarify the correlation, if any, between carriers and the mechanism of ferromagnetic inherent to this class of diluted magnetic semiconductors. On the other hand, defects are supposed to play a primary role on ferromagnetic ordering in transition-metal ZnO **[18-21]**. Song et al. **[42]** found that in Co-doped ZnO is strongly correlated with structural defects. In their case, these defects are introduced by increasing carriers (electron concentration). On the other hand, an insulating nature in these diluted magnetic materials especially Co-doped ZnO is significant in a magnetic coupling interaction other than carrier-mediated exchange which is apparently operative. So again, defects, which are also normally caused by incorporation of dopants, play an important role in the system. An electron associated with a particular defect confined in a hydrogenic orbital comes with dielectric constant as found by Song et al. **[43]**. Hence high dielectric constant results in large hydrogenic orbital radius. This is consistent with our results presented in Fig. 9, which indicate that the increase in in RTFM is induced by

increasing in refractive index. Therefore, according to the Raman results and ref. **[43],** this can be attributed to the structural disordering caused by ion (Mn in our case) incorporation. This will mean that the paramagnetic films (Mn:ZnO) are transparent to UV light and become opaque when are ferromagnetic.

Fig. 8 shows the refractive index (n) and extinction coefficient (k) as function of Mn concentration. It is evident that the n decrease for both films (thinner and thicker), while the k increases with increasing the Mn concentration in the ZnO matrix. There is a hump indicated by an arrow in both films (Fig. 8a and b) for the extinction coefficient (k). This hump is observed at the same concentration of 0.25 at.% of Mn for both thinner and thicker films. However, the origin and interpretation of this observation will be discussed later in the paper.

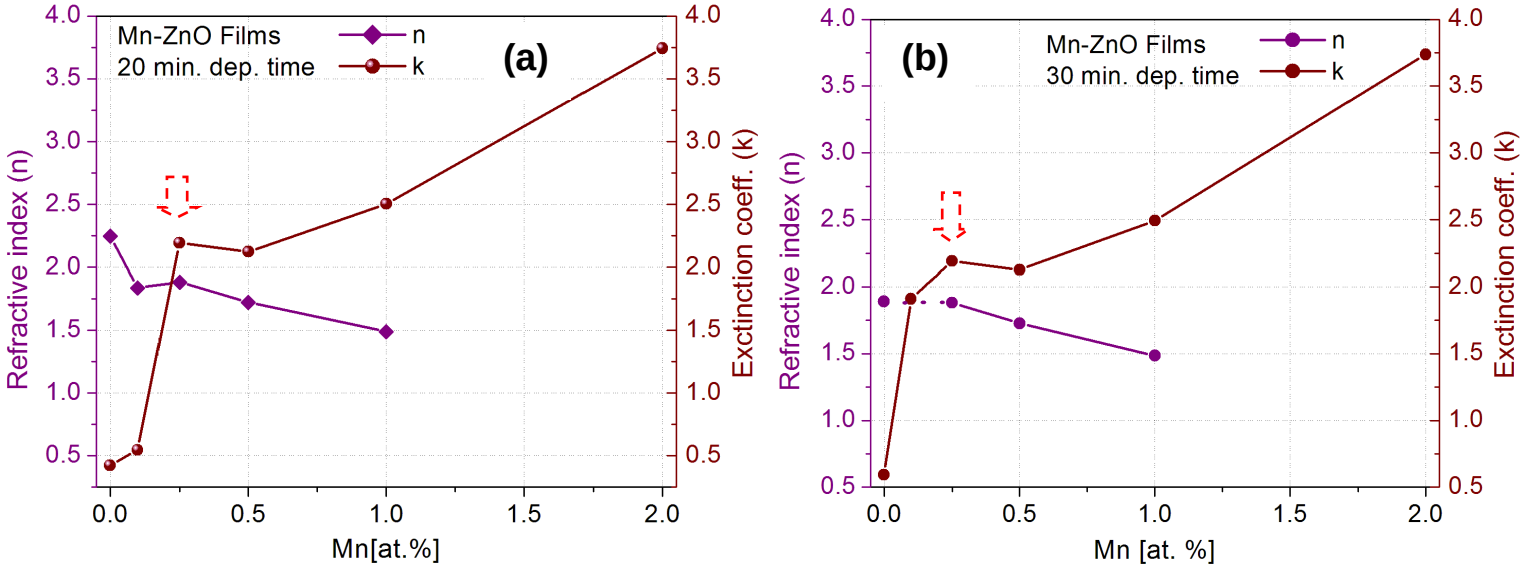

Fig. 8: The dependence of optical constants, n and k, with Mn concentration for the (a) thinner and (b) thicker films.

The optical constants show some interesting correlation with the FMR spins origin. Fig. 9a and b show the dependence of n and k on the ferromagnetic ordering in terms of its intensity, number of spins for both thinner and thicker films, respectively. It is very fascinating to note that both films show that the refractive index (n) increases with ferromagnetic ordering while extinction coefficient (k) reduces. This suggests that when the Mn:ZnO films become more opaque (high reflectance) to UV (~ 370 nm) and absorbs less of that light, the RTFM ordering is enhanced. Again, if that is the case, it would also mean that super-paramagnetic films are more transparent to UV light.

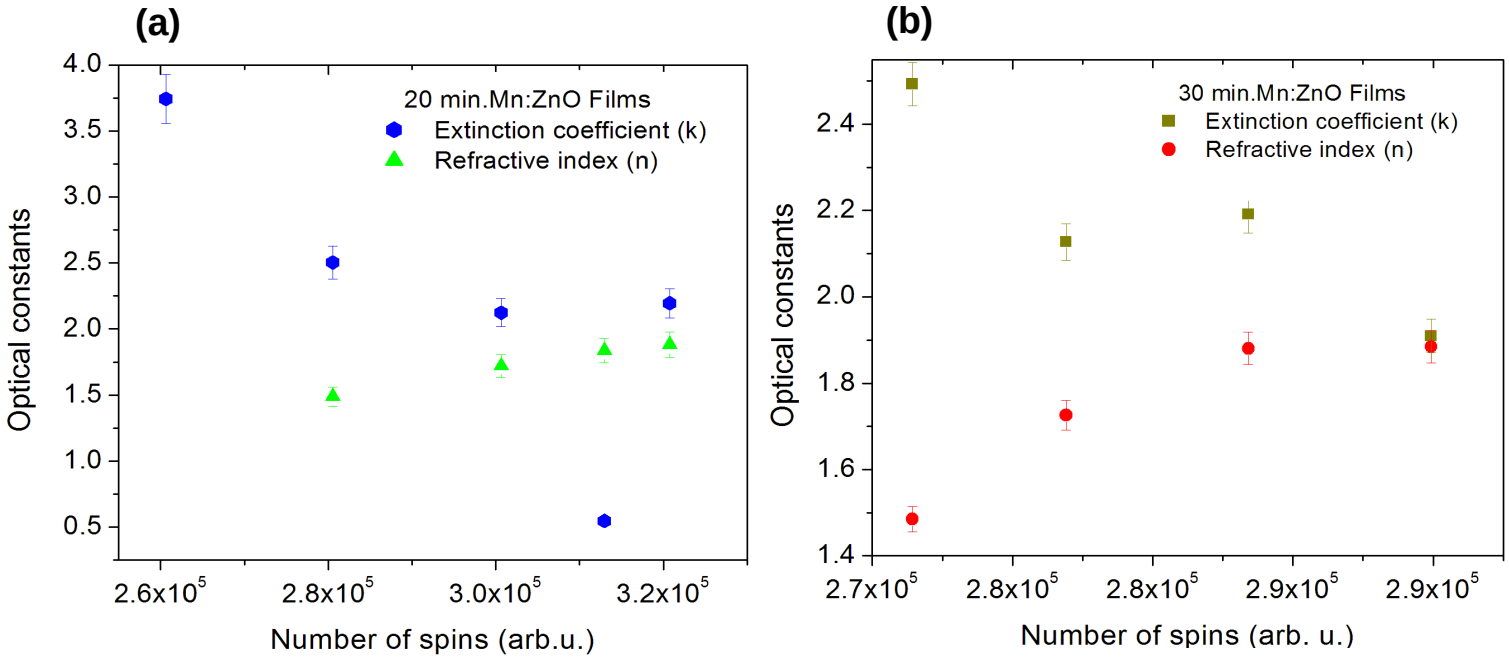

Fig. 9: The dependence of optical constants with the number of ferromagnetic spins for both (a) thinner and (b) thicker Mn:ZnO films.

To further elucidate in detail the effect of Mn doping on the ZnO, we carried out effective medium approach (EMA) for inhomogeneous materials. In keeping up with our data the eq. 1 can be re-written as follows:

$$\delta_{Mn}\frac{\varepsilon_{Mn}-\varepsilon_{eff}}{\varepsilon_{Mn}+\varepsilon_{eff}}+\left(1-\delta_{Mn}\right)\frac{\varepsilon_{ZnO}-\varepsilon_{eff}}{\varepsilon_{ZnO}+\varepsilon_{eff}}=0 \qquad (4)$$

Only two components Mn and ZnO are considered here. Solving for ε_{eff} results into two possible solutions as:

$$\varepsilon_{eff}=\frac{1}{2}\left(2\delta\varepsilon_{Mn}-\varepsilon_{Mn}+\varepsilon_{ZnO}-2\delta\varepsilon_{ZnO}-\sqrt{4\varepsilon_{Mn}\varepsilon_{ZnO}+\left(2\delta\varepsilon_{Mn}-\varepsilon_{Mn}+\varepsilon_{ZnO}-2\delta\varepsilon_{ZnO}\right)^2}\right),$$

$$\varepsilon_{eff}=\frac{1}{2}\left(2\delta\varepsilon_{Mn}-\varepsilon_{Mn}+\varepsilon_{ZnO}-2\delta\varepsilon_{ZnO}+\sqrt{4\varepsilon_{Mn}\varepsilon_{ZnO}+\left(2\delta\varepsilon_{Mn}-\varepsilon_{Mn}+\varepsilon_{ZnO}-2\delta\varepsilon_{ZnO}\right)^2}\right)$$

In terms of the more fundamental optical properties of ZnO, there have been a number of comprehensive studies to determine the refractive index and dielectric constant of this material **[19, 44-46]**. The measurements were all carried out using spectroscopic ellipsometry technique. Plotting the effective dielectric properties shown in Fig. 10 solution under any given concentration values, it shows that the dielectric properties decrease with increasing concentration. This agrees well with our curves in Fig. 8 especially for the refractive index.

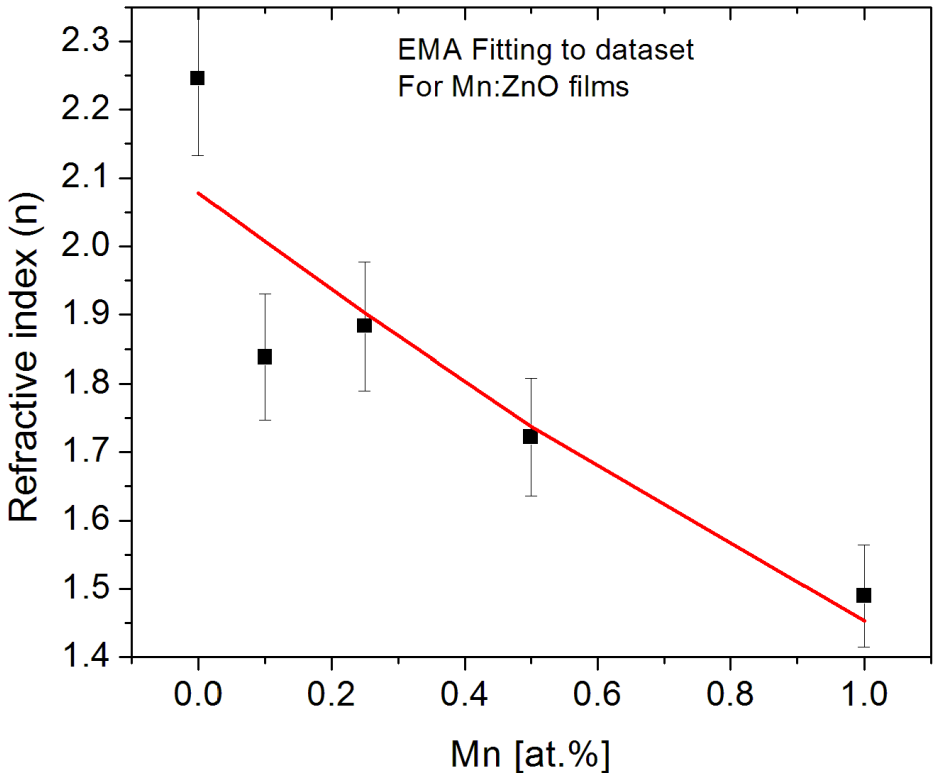

Fig. 10: Mathematica plot fit. An application of the effective medium approach to our experimental data points to extract parameters. The δ_{Mn} concentration fraction can go up 100% atomic percentage depending on experimental condition. The Mn doping in our case could go up to 1 at.%.

This agrees well with Lichteneker's empirical logarithmic mixing rule equation **[47]** often employed by other workers **[48]** to mix, the dielectric properties of mixtures of varying proportions mixed at room temperature decreases with amount concentration added. In order to understand a decreasing behaviour observed from refractive index, mathematica software was used to do a non-linear-model fit in our experimental data. Therefore, by using the EMA model, the values of n for both ZnO and Mn were obtained as shown in Table 2. These values are in good agreement with the ones observed from the literature **[17, 44-46]**.

Table 2: Summary of dielectric constant for ZnO and Mn.

	Estimate	Std error	t-Statistics	P-Value	R^2
ε_{ZnO}	2.11095	0.351447	6.00644	0.00924475	0.996589
ε_{Mn}	4.31666	0.390812	11.0454	0.00158951	

The dielectric constant (ε) is normally composed of real (ε) and complex (ε) given as follows:

$$\varepsilon = \varepsilon_{real} + i\varepsilon_{complex} = (n + ik)^2 \tag{5}$$

Expanding eq. 5 further leads to:

$$\varepsilon = \varepsilon_{real} + i\varepsilon_{complex} = n^2 + 2ink - k^2 \tag{6}$$

This will mean that;

$$\varepsilon_{real} = n^2 - k^2 \text{ ; and } \varepsilon_{complex} = 2nk \tag{7}$$

Therefore with some simplification the refractive index (n) and extinction coefficient (k) are given by:

$$n = \left(\frac{\sqrt{\varepsilon_{real}^2 + \varepsilon_{complex}^2} + \varepsilon_{real}}{2} \right)^{1/2} ; k = \left(\frac{\sqrt{\varepsilon_{real}^2 + \varepsilon_{complex}^2} - \varepsilon_{real}}{2} \right)^{1/2} \tag{8}$$

The EMA model from Bruggeman nor Maxwell-Garnet cannot justify the hump noticed on the extinction coefficient (k) with Mn concentration (Fig. 7a and b). The

only possible and accurate answer could be found in Drudel model of the optical properties of metals. The model does not only explain the appearance of the hump but also explains a possible shift in energy of photon for different metals. Such behaviour is only noticed in transition-metal compounds and is said to be due to a *d*-band resonance at about 3.351 eV (~370 nm). The *d*-band lie below the Fermi energy of the conduction band: fairly narrow band of energies, around $\hbar\omega_0 = E_F - E_d$ which can be modelled as additional Lorentz oscillator. The combined effects of the free-electrons (Drude model) and the inter-band transitions due to bound *d*-electrons (Lorentz model) influence the reflectance properties of the metal **[49]**. Reddy et al. **[50]** showed that the reflectance of Cu co-doped samples decreased with increase in Cu concentration.

4. CONCLUSION

We have successfully synthesized Mn:ZnO films of novel structures using aerosol spray pyrolysis at different deposition times. Magnetic properties of Mn:ZnO films revealed ferromagnetic ordering with some low-field magnetic absorption observed in certain concentration of Mn. The effect of Mn concentration on the FMR intensity signal and its width was successfully studied. The angular dependence of this latter was studied. The results revealed that Mn concentration seems to directly affect the dielectric constants the same way as the FMR width showing that the refractive index decreases (including the width) as a function of Mn concentration. The obtained dielectric constants were correlated with the ferromagnetic ordering. The effect of Mn carrier concentration to ferromagnetic ordering was also studied. A *d*-band resonance at 3.35 eV was found in these Mn:ZnO films at 0.25 at.% Mn

which was due to the transition-metal. Bruggeman EMA model was also used in an attempt to explain the variation of the dielectric properties (real and complex part), and the model fit was successfully correlated with the dielectric constant for ZnO and Mn.

5. ACKNOWLEDGEMENTS

This work was supported by the Department of Science and Council for Scientific and Industrial Research (Project Numbers: LHIE100, HGER28P and HGER27S) and WIROX project (PIRSES-GA-2011-295216), a Marie Curie International Research Staff Exchange Scheme Fellowship within the 7th European Community Framework Programme and 'ORAMA': Oxide Materials Towards a Matured Post-silicon Electronics ERA FP7-NMP - CONTRACT N°: 246334. S.S. Nkosi wishes to acknowledge the SERA project (HGER29X) for the traveling costs. The authors are also thankful to the equipment supplied by the NCNSMs and FORTH institute for the analysis.

6. REFERENCES

[1] X.Y. Mao, W. Zhong, Y.W. Du, Journal of Magnetism and Magnetic Materials 320 (2008) 1102.

[2] I. Zutic, J. Fabian, S.D. Sama, Reviews of Modern Physics 76 (2004) 323.

[3] C. Jing, Y. Jiang, W. Bai, J. Chu, A. Liu, Journal of Magnetism and Magnetic Materials 322 (2010) 2395.

[4] E. Chikoidze, Y. Dumont, H.J. Bardeleben, W. Pacuski, O. Gorochov, Superlattices and Microstructures 42 (1-6) (2007) 176.

[5] R.Q. Wu, G.W. Peng, L. Liu, Y.P. Feng, Z.G. Huang, Q.Y. Wu, Appl. Phys. Lett. 89 (2006) 062505.

[6] T. Dietl, H. Ohno, F. Matsukura, J. Cibert, D. Ferrand, Science 287 (2000) 1019.

[7] K. Ueda, H. Tabata, T. Kawai, Appl. Phys. Lett. 79 (7) (2001) 988.

[8] Y.Q. Wang, S.L. Yuan, L. Liu, P. Li, X.X. Lan, Z.M. Tian, J.H. He, S.Y. Yin, J. Magnetism and Magnetic Materials 320 (2008) 1423.

[9] H. Saeki, H. Tabata, T. Kawai, Solid State Communications 120 (11) (2001) 439.

[10] P. Sharma, A. Gupta, K.V. Rao, F.J. Owens, R. Sharma, R. Ahuja, J.M.O. Guillen, B. Johansson, G.A. Gehring, Nature Materials 2 (2003) 673.

[11] P. Sharma, A. Gupta, F.J. Owens, A. Inoue, K.V. Rao, J. Magnetism and Magnetic Materials 282 (2004) 115.

[12] H. Hori, S. Sonoda, T. Sasaki, Y. Yamamoto, S. Shimizu, Ken-inchi Suga, K. Kindo, Physica B 324 (2002) 142.

[13] D.P. Norton, S.J. Pearton, A.F. Hebard, N. Theodoropoulou, L.A. Boatner, R. G. Wilson, Appl. Phys. Lett. 82 (2003) 239.

[14] K.R. Kittilstved, N.S. Norberg, D.R. Gamlin, Phys. Rev. Lett. 94 (2005) 147209.

[15] S.S. Kim, J.H. Moon, B.-T. Lee, Oh S. Song, J Ho Je, J. Appl. Phys. 95 (2004) 454.

[16] T. Fukumura, Z. Jin, M. Kawasaki, T. Shono, T. Hasegawa, S Koshihara, H. Koinuma, Appl. Phys. Lett. 78 (2001) 958.

[17] A. Tiwari, C. Jin, A. Kvit, D. Kumar, J.F. Muth, J. Narayan, Solid State Communications 121 (2002) 371.

[18] X. Xu, C. Xu, J. Dai, J. Hu, Fengji Li, S. Zhang, J. Physical Chemistry C 116 (2012) 8813.

[19] J.M.D. Coey, M. Venkatesan, C.B. Fitzgerald, Nat. Mater. 4 (2005) 173.

[20] Y.B. Zhang, Q. Liu, T. Sritharan, C.L. Gan, S. Li, Appl. Phys. Lett. 89 (2006) 042510.

[21] T.S. Herneg, S.P. Lau, S.F. Yu, H.Y. Yang, X.H. Ji, J.S. Chen, N. Yasui, H. Inaba, J. Appl. Phys. 99 (2006) 086101.

[22] W. Prellier, A. Foucher, B. Mercy, J. Phys.: Condens. Matter. 15 (2003) R1583

[23] S.J. Pearton, D.P. Norton, M.P. Ivill, A.F. Hebard, J.M. Zavada,. W.M. Chen, I.A. Buyanova, J. Electron. Mater. 36 (2007) 462.

[24] D. Stroud, Phys. Rev. B 12 (1975) 3368.

[25] G. Kenanakis, Z. Giannakoudakis, D. Vernardou, C. Savvakis, N. Katsarakis, Catalysis Today 151 (2010) 34.

[26] I. Kortidis, K. Moschovis, F.A. Mahmoud, G. Kiriakidis, Thin Solid Films 518 (2009) 1208.

[27] G. Kiriakidis, K. Moschovis, I. Kortidis, V. Binas, Vacuum 86 (2012) 495.

[28] R.J. Lang, J. Acoust. Soc. Am. 34 (1962) 6.

[29] W. Thomson (Kelvin), Philos. Mag. 42, 448 (1871).

[30] J.A. Woollam Inc. Complete Ease^{TM} Data Analysis Manual, June 15 2008.

[31] B. Johs, J.S. Hale, Phys. Status Solidi A 205 (2008) 715.

[32] D.E. Motaung, G.F. Malgas, C.J. Arendse, S.E. Mavundla, Mater. Chem. Phys. 135 (2012) 401.

[33] D.E. Motaung, G.H. Mhlongo, I. Kortidis, S.S. Nkosi, G.F. Malgas, B.W. Mwakikunga, S. Sinha-Ray, G. Kiriakidis, Applied Surface Science (2013) submitted for publication.

[34] D. Perednis, L.J. Gauckler, J. Electroceramics 14 (2005) 103.

[35] L.A. Patil, A.R. Bari, M.D. Shinde, V. Deo, Sensors and Actuators B 30 (2010) 290.

[36] S.S. Nkosi, I. Kortidis, D.E. Motaung, G.H. Mhlongo, G.F. Malgas, J. Keartland, E. Sideras-Haddad, A. Forbes, B.W. Mwakikunga, S. Sinha-Ray, G. Kiriakidis, J. Alloys and Compounds (2013) accepted.

[37] S.S. Nkosi, B. Yalisi, D.E. Motaung, J. Keartland, E. Sideras-Haddad, A. Forbes, B.W. Mwakikunga, Appl. Surf. Sci. 265 (2013) 860.

[38] Usman, Ilyas, R.S. Rawat, Y. Wang, T.L. Tan, P. Lee, R. Chen, H.D. Sun, Fengji Li, Sam Zhang, Appl. Surf. Sci. 258 (2012) 6373.

[39] Y.-H. Lin, M. Ying, M. Li, X. Wang, X. Wang, C.-H. Nan, Appl. Phys. Lett. 90 (2007) 222110.

[40] N.H. Hong, V. Brize, J. Sakai, Appl. Phys. Lett. 86 (2005) 082505.

[41] M. Ivill, S.J. Pearton, Y.W. Heo, J. Kelly, A.F. Hebard, D.P. Norton, J. Appl. Phys. 101 (2007) 123909.

[42] C. Song, S.N. Pan, X.J. Liu, X.W. Li, F. Zeng, W.S. Yan, B. He, F. Pan, J. Phys.: Condens. Matter 19 (2007) 176229.

[43] C. Song, K.W. Geng, F. Zeng, X.B. Wang, Y.X. Shen, F. Pan, Phys. Rev. B 73 (2006) 024405.

[44] H. Yoshikawa, S. Adachi, Jpn. J. Appl. Phys. 36 (1997) 6237.

[45] N. Ashkenov, B. M. Mbenkum, C. Bundesmann, V. Riede, M. Lorenz, D. Spemann, E. M. Kaidashev, A. Kasic, M. Schubert, M. Grundmann, G. Wanger, H. Neumann, V. Darakchieva, H. Arwin, B. Monemar, J. Appl. Phys. 93 (2003) 126.

[46] X.W. Sun, H. S. Kwok, J. Appl. Phys. 86 (1999) 408.

[47] K. Lichteneker, Physik. Z., 27 (1926) 115.

[48] N.H. Langton, A.M.Brit.I.R.E., A.Inst.P., D. Matthews, A.N.C.R.T., D.P.I., Br. J. Appl. Phys. 9 (1958) 453.

[49] D.J. Hagan and P.G. Kik, OSE5312-Light Matter Interaction, CREOL, The College of Optics and Photonics, University of Central Florida, (2011) pp.52.

[50] D.A. Reddy, G. Murali, B. Poornaprakash, R.P. Vijayalakshmi, B.K. Reddy, Appl. Surf. Sci. 258 (2012) 5206.

FIGURE CAPTIONS AND TABLES

Table 1: Summary of Raman modes of Mn doped ZnO nanostructures with thinner and thicker films.

Table 2: Summary of the estimated dielectric constant for ZnO and Mn.

Fig. 1: The optical microscope images for the Mn (2 at.%) doped ZnO structures with different films (a) thinner and (b) thicker films.

Fig. 2: Polarized optical microscope images of Mn doped ZnO structures of thin (a-c) and thick films (d-f). The Mn concentrations used were 0.1, 0.5 and 1at.% for both thinner and thicker films.

Fig. 3: SEM micrographs of (a) undoped ZnO with a thinner film, (b) 0.1at.%, (c) 1at.% Mn doped ZnO with thinner films; (d) undoped ZnO with a thicker film, (b) 0.1at.%, (c) 1at.% Mn doped ZnO with thicker films.

Fig. 4: EBS-Detector micrographs of Mn doped ZnO (1 at.%) with thinner and thicker films deposited for (a) 20 min and (b) 30 min indicate different phases on the surface of Mn:ZnO films.

Fig. 5: Raman spectra of Mn:ZnO films at various concentration of Mn for both (a) thinner and (b) thicker deposited films respectively.

Fig. 6: The dependence of RTFM intensity and peak-to-peak width at various Mn concentrations (a) magnetic field parallel to the film and (b) when the magnetic field is perpendicular to the film. It should be pointed out that (a-b) correspond to the thinner films deposited for 20 min and (c-d) thicker films deposited for 30 min.

Fig. 7: The dependence of number of spins (N_s) of the ferromagnetic ordering as a function of Mn concentration.

Fig. 8: The dependence of optical constants, n and k, with Mn concentration for the (a) thinner and (b) thicker films.

Fig. 9: The dependence of optical constants with the number of ferromagnetic spins for both (a) thinner and (b) thicker Mn:ZnO films.

Fig. 10: Mathematica plot fit. An application of the effective medium approach to our experimental data points to extract parameters. The δ_{Mn} concentration fraction can go up 100% atomic percentage depending on experimental condition. The Mn doping in our case could go up to 1 at.%.